



OPEN

Extreme tunability in aluminum doped Zinc Oxide plasmonic materials for near-infrared applications

SUBJECT AREAS:
OPTICS AND PHOTONICS
MATERIALS FOR OPTICSReceived
5 June 2014Accepted
1 September 2014Published
18 September 2014Correspondence and
requests for materials
should be addressed to
A.K.P. (apradhan@
nsu.edu)A. K. Pradhan¹, R. M. Mundle¹, Kevin Santiago¹, J. R. Skuza¹, Bo Xiao¹, K. D. Song¹, M. Bahoura¹, Ramez Cheaito² & Patrick E. Hopkins²¹Center for Materials Research and Department of Engineering, Norfolk State University, 700 Park Avenue, Norfolk, VA 23504, ²Department of Mechanical and Aerospace Engineering, University of Virginia, 122 Engineer's Way, Charlottesville, VA 22904-4746.

Plasmonic materials (PMs), featuring large static or dynamic tunability, have significant impact on the optical properties due to their potential for applications in transformation optics, telecommunications, energy, and biomedical areas. Among PMs, the carrier concentration and mobility are two tunable parameters, which control the plasma frequency of a metal. Here, we report on large static and dynamic tunability in wavelengths up to 640 nm in Al-doped ZnO based transparent conducting degenerate semiconductors by controlling both thickness and applied voltages. This extreme tunability is ascribed to an increase in carrier concentration with increasing thickness as well as voltage-induced thermal effects that eventually diminish the carrier concentration and mobility due to complex chemical transformations in the multilayer growth process. These observations could pave the way for optical manipulation of this class of materials for potential transformative applications.

The resonant frequency of plasmonic materials (PMs) can be tuned over a range¹ by controlling the dielectric medium. This can produce new functional devices in which the optical response of can be engineered by manipulating designs and composition of currently studied metamaterials, where their unique optical properties are not seen in individual components²⁻⁵. The tuning of the resonant frequency in many PMs is achieved by carrier injection in semiconductors⁶, mechanical reorientation in microelectromechanical systems⁷, varying the dielectric environment⁸, and many other emerging phenomena. The recent report⁷ on a tunability of compliant metamaterials using high-strain mechanical deformation between the resonant elements in coupled resonators has drawn tremendous interest and shown a pathway for imminent applications. However, although the expensive manufacturing of complex large-volume and low-loss tunable PMs is still a formidable challenge in itself⁹, and may easily expand in new inexpensive directions to find applications if their tunability is either controlled by applying an electric field or varying the thickness of the materials. The onset of interband transition is 3.9 eV for Ag and 2.3 eV for Au, which is in the ultraviolet or green light, far way from the near infrared (NIR) which is the interest of materials being developed in this work.

The Fermi level (E_f), for some of the transparent conducting oxides (TCOs) known as degenerate semiconductors, is found within the conduction band (CB) or above the conduction band (E_c), as is found in a metal. For example, such is the case when the wide bandgap semiconductor ZnO is doped with either Ga or Al. These doped semiconductors demonstrate properties that are more metal than semiconductor-like with the resistivity, (ρ) being proportional to the temperature, (T). Doped (Ga or Al) ZnO based TCOs have shown the above electrical dependence and generic n-type behavior with high carrier concentrations¹⁰⁻¹². This class of semiconductor materials demonstrates remarkable properties of low-loss PMs¹³⁻¹⁷ because semiconductors do not have bound-state absorption transitions in their band-gaps, and their surface plasmon polariton losses can be even smaller, in the NIR region than those with conventional plasmonic materials at corresponding visible wavelengths¹⁸. However, no significant tuning of the resonant frequency in this class of PMs^{16,19-21} has been achieved by varying different conditions, such as growth, doping concentration, etc. We demonstrate that the crossover wavelength (λ_c) can be widely tuned by varying the thickness of the layers, as well as by dynamically controlling the electric field on the surface of the films in this degenerate semiconductor.



Results

The Al-doped ZnO (AZO) thin films with varying thickness and multilayers comprising of different Al:Zn composition ratios were grown via alternate deposition of diethyl zinc (DEZ, $\text{Zn}(\text{C}_2\text{H}_5)_2$), H_2O and trimethylaluminum (TMA, $\text{Al}(\text{CH}_3)_3$) through atomic layer deposition (ALD) cycles²² (see supplementary information). ALD is used to attain conformal and pinhole-free films with a high degree of thickness control. The sequential exposure of reactants used in ALD adjusts the composition of multicomponent materials by changing the number of cycles used for each precursor materials (See schematics in Supplementary Fig. 1a). Variable angle spectroscopic ellipsometry (VASE) (see supplementary information) was used to measure the λ_c from positive to negative permittivity using the Drude-Lorentz model. Fig. 1a demonstrates the crossover of the real permittivity from positive to negative as the thickness of AZO films is varied from 69 to 577 nm. The corresponding imaginary permittivity (loss) is illustrated in Fig. 1b. The thickness dependence of λ_c is found to fall exponentially as the thickness of the films increases (Fig. 1c). While tunability of a PM is very desirable for device applications, tuning by manipulating the thickness could prove to be of particular importance for the fabrication of real devices. We found that the λ_c is significantly tunable with a range of 640 nm in the NIR region by simply changing the thickness of AZO films. While this large range of tunability is observed in the NIR range, the loss is significantly diminished as the thickness increases

(Fig. 1b) due to higher conductivity in the thicker films. Moreover, the dispersion in the imaginary part of the permittivity is significantly less over the measured range.

If we consider the plasma frequency of the film (ω_p), which is defined by equation (1):

$$\omega_p^2 = \frac{n_e e^2}{\epsilon_0 m_0} \quad (1)$$

and is related to the real part of the permittivity by the following equation (2):

$$\epsilon(\omega)' + i\epsilon(\omega)'' = \epsilon(\omega) = \epsilon_{int} - \frac{\omega_p^2}{\omega(\omega + i\Gamma)} \quad (2)$$

where n_e is the carrier concentration, m_0 is the effective mass, ϵ_{int} is the permittivity due to interband transitions, and ϵ_0 and e^2 are the free-space permittivity and electron charge, respectively. In eq. (2) Γ is the total damping rate. The plasma frequency is directly proportional to the carrier concentration. It is also noted that the real permittivity should be negative for plasmonic materials. Fig. 1c shows the AZO film thickness and the corresponding calculated carrier concentration for the corresponding λ_c , while Fig. 1d shows the experimental carrier concentration, and sheet carrier density, n_s , with increasing thickness of the AZO films. The sheet carrier density was calculated from the Hall voltage. The trend of λ_c dependence on

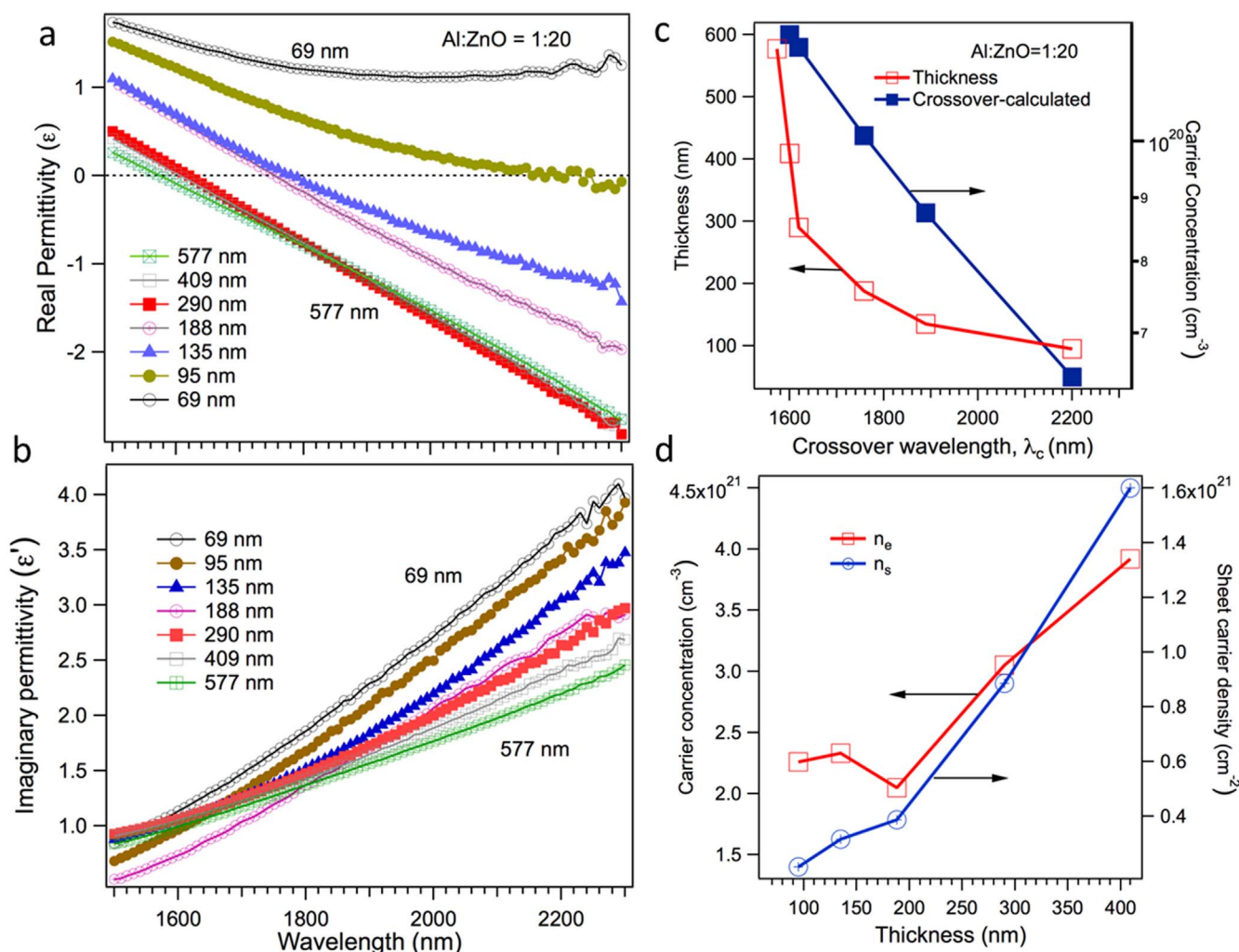


Figure 1 | Room temperature permittivity and carrier concentrations. Wavelength dependence of the (a) real and (b) imaginary permittivity of Al: ZnO (1: 20 ratio) films containing low (69 nm) to higher (577 nm) thickness. (c) Thickness dependence of crossover wavelength, λ_c , and calculated carrier concentration using the Drude-Lorentz model. (d) Dependence of measured carrier concentration (n_e) and sheet carrier density (n_s) of AZO films.



thickness can be related to the enhanced carrier concentration and sheet carrier density of the films, which validates the plasma frequency relation with carrier concentration in Eq. (1). Although the carrier concentration in Fig. 1c and d is slightly different, the discrepancy is due to the two separate techniques, such as carrier concentration calculated numerically using eq. (1) and λ_c for Fig. 1c and experimentally using Hall configuration for Fig. 1d. There is a large change in the resistivity going from as high as $1.19 \times 10^{-3} \Omega\text{-cm}$ for the 69 nm film down to as low as $7.9 \times 10^{-4} \Omega\text{-cm}$ for the 577 nm thick film. The metal-like behavior is noted for films with higher thickness (see supplementary information), which is basically due to Al donor electrons filling up the lower levels in the conduction band as seen in degenerate semiconductors. The columbic interactions between the positively charged metal ions are minimized in the ALD process^{23–25} by keeping the Al dopants as far apart as possible, which makes this process unique for controlling the carrier concentration. As we increase the number of macrocycles, the projected surface area is expected to increase²⁶. This provides an enormous opportunity for passively tuning the PM devices during the ALD fabrication process by spatially varying the thickness, and hence the carrier density.

Figure 2a and b show the wavelength dependence of the real and imaginary permittivity with applied voltage, respectively, for the gradient sample, G1, in which the electron concentration is varied

from bottom to top (Fig. 2c inset (See Supplementary Fig. 1b and c)). The wavelength dependence of the real and imaginary permittivity with applied voltages are also shown for two sample thicknesses, 100 and 150 nm with Al:Zn=1:20. The electric field controlled permittivity is an excellent method to dynamically control the plasmonic properties of AZO films. The λ_c of a specially designed multilayer AZO thin film (G1 gradient sample) in which the Al-content was varied along the thickness of the film (See Supplementary Fig. 1b and c) can be tuned up to 450 nm by simply applying a voltage on the sample as shown in Fig. 2c, thus demonstrating an electric field controllable plasmonic metamaterial for potential device applications with reasonably low loss at higher applied voltages (Fig. 2b). However, a contrasting effect is that λ_c does not show reversible behavior beyond the applied voltage of 12 V. Since these measurements combine both incident light and applied electric field, this observed effect may be related due to electro-absorption in a material, a phenomenon called the Franz-Keldysh effect^{27,28}, that occurs in low-dimensional systems, such as quantum wells, quantum wires, and quantum dots due to quantum confinement effects^{29,30}. In order to verify the Franz-Keldysh effect (see supplementary information) in these AZO samples, electro-absorption experiments were performed on the 577 nm thick films with applied voltages up to 12 V over the 300 to 2000 nm wavelength range for the incident light. No significant difference in electro-absorption characteristics

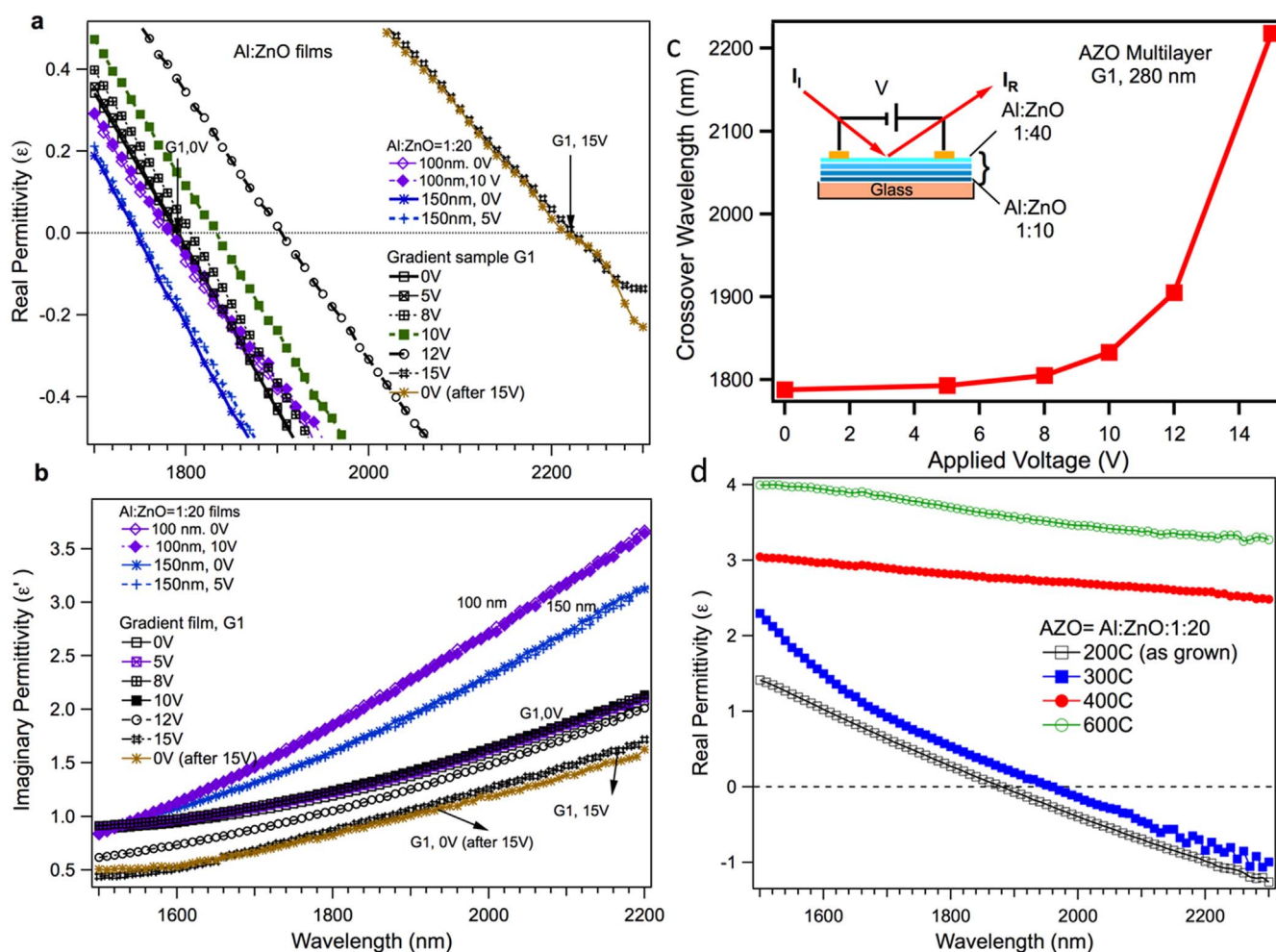


Figure 2 | Room temperature permittivity and carrier concentrations. Wavelength dependence of the (a) real and (b) imaginary permittivity of Al:ZnO (1:20 ratio) films (100 and 150 nm) and gradient film, G1 (280 nm) at various applied voltages. Results are also shown for no applied voltage after the 15 V measurements, which exhibit irreversibility. (c) Applied voltage dependence of crossover wavelength, λ_c for the multilayer G1 film, where the Al:ZnO ratio varies from 1:10 to 1:40 (Supplementary Fig. 1). (d) Wavelength dependence of the real permittivity of 150 nm thick Al:ZnO (1:20 ratio) films annealed at various temperatures after growing at 200°C.



was observed (Fig. 5 and supplementary information) in our experiments, which implies that the Franz-Keldysh effect has no significant influence on our AZO films.

In order to explore the reasons for this dynamic voltage induced tuning, some of the samples were annealed at various temperatures. The λ_c changed from 1878 to 1963 nm for the 150 nm thick as-grown films annealed at 300°C (Fig. 2d). However, for annealing temperature greater than 400°C, no trend of the real permittivity crossover was seen as is clearly shown in Fig. 2d, providing evidence that the number of free charge carriers has diminished³¹ according to Eq. (1) for films annealed at temperatures higher than 300°C. The above consequence provides a clear sign that the films are undergoing morphological changes, which impact the carrier concentration in the films.

In order to further investigate the reasons for dynamic electrical tunability, we performed a series of time-dependent electro-thermal experiments. While a specific voltage was applied onto the sample surface using deposited metal electrode pads, the temperature and current developed between the contacts were monitored over time as shown in Fig. 3 from 10 to 20 V for AZO films with thickness of 577 nm. Interestingly, a temperature rise to 325°C can be reached as the voltage increases to 20 V, similarly to 140 and 300°C for 10 and 15 V, respectively. The current follows a similar trend as the temperature, except that it falls off sharply as the voltage supply is ceased. Additionally, the temperature rise time is much faster for higher voltages than for lower ones. The ellipsometry measurements were performed by applying voltage on the samples for a duration of 8 to 10 h. This causes a Joule heating effect, which we have evidenced from precise thermal conductivity and electrical property measurements of the AZO films. The Joule heating effect is supported by the observed metallic behavior in temperature dependent electrical transport of these films (See Supplementary Fig. 2b and c). Thermal conductivity of AZO films was measured by the time-domain thermoreflectance (TDTR) technique³² (Supplementary Fig. 3), and the thermal conductivity was found with moderate value for the AZO films. For example, the room-temperature thermal conductivity for an AZO sample with thicknesses of 290 nm is 4.264 ± 0.11 W/m/K, and for the gradient sample (287 nm thick) it is 5.65 ± 0.38 W/m/K. TDTR measurements were performed at higher temperatures. The thermal conductivities are relatively constant from room temperature to 373K (supplementary information under thermal conductivity). This is explained in the framework of better metallic behavior observed in these samples (Supplementary Fig. 2), especially in thicker films. We also noticed higher heat generation due to Joule heating in thicker films (inset of Fig. 3). The moderate thermal conductivity in AZO films facilitates heat transport along the film, which causes the temperature to rise above 300°C at higher applied voltages. Prolonged applications at higher voltages raise the temperature to a level where the films get annealed, thus diminish the carriers.

The temperature distribution was recorded with an infrared camera over a 1 cm² area of the AZO film. The gradual rise of the temperature is imaged and their corresponding temperature profiles are shown in Fig. 4 A, and B, respectively. These observations confirm that λ_c varies with the applied voltages, which produce thermal effects over the entire films, especially between the contact pads. It is noted that all the areas on the glass substrate except the square region (1 cm²) containing AZO film shown in Fig. 4A is etched out. Hence the heat dissipates from the film to the substrate underneath and the surrounding area. These results indicate that the voltage induced thermal effect is associated with the unique layer-by-layer structure of the films.

Recent cross-sectional microscopic studies revealed that ALD-grown AZO films are formed by a unique layer-by-layer structure, which is better explained as a nanolaminate structure, of a ZnO matrix and Al₂O₃ dopant layers^{25,33}, where free electrons are pro-

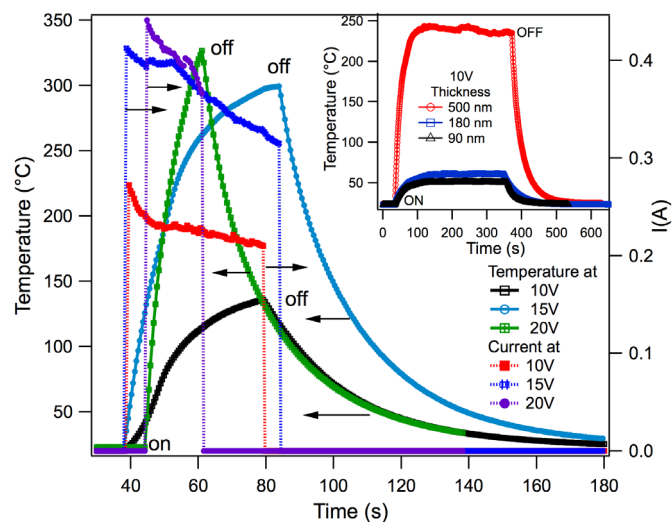


Figure 3 | Thermal effects due to applied voltages. The heat is generated due to applied voltages, and both on and off conditions are shown. The current (dotted lines) sharply rises with the applied voltages when switched on and suddenly falls off to zero when switched off. The samples cool down exponentially after the voltage is turned off. The inset shows the rise and fall of temperature with time for various film thicknesses for both on and off voltage cases.

vided to the ZnO matrix by the Al₂O₃ dopant layers. Due to the increased temperature, at the higher applied voltages, the local Al₂O₃ dopant layers form AlO_x islands that cause interface scattering. This scattering reduces the mobility at the grain boundaries and decreases the carrier concentration, which is similar to the effects of annealing seen in ALD-grown AZO films³¹. Consequently, the decrease in carrier concentration shifts λ_c to a higher wavelength region, and finally the dielectric permittivity becomes positive due to a loss of carriers responsible for metallic behavior. The reversible tunability up to 12 V of applied voltage corroborates the fact that the thermomorphological transformation is limited as shown in Fig. 2d for thermally annealed ALD-grown AZO films. However, above 12 V significant chemical and morphological transformation occurs due to nanolaminate structures forming AlO_x-based electron trapping centers as well as severe interface scattering. Due to the wide tunability of λ_c , there is enough scope for these ALD-grown AZO films for telecommunication applications in the NIR region by fabricating suitable waveguides. The present experimental results clearly demonstrate the passive and dynamic fine tunability of AZO films due to the interplay of carriers and electro-thermal properties forming a transparent heater. The Joule heating ($P=I^2R$, where I is current, and R is resistance) due to applied voltage gets saturated after a few seconds and dissipates after switching off the voltage. As the applied voltage is proportional to the current that develops, a larger heating effect is observed at higher applied voltages. At the same time, thicker films produce a much larger heating effect compared to thinner films due to higher carriers. This is due to generation of larger currents in thicker films as the progressive increase of current is seen with the increase of voltages as well as the thickness of the films. Further analysis should provide more insight into the details of the mechanism behind these novel findings.

Methods

Fabrication of Al doped ZnO. The Al-doped ZnO (AZO) samples were prepared using a Cambridge Nanotech Savannah 100 atomic layer deposition (ALD) system. The base pressure of the ALD system was 5.2×10^{-3} Torr and increased to 1.7×10^{-1} Torr with ultra-high purity N₂ inert carrier gas flowing through at 20 SCCM. The AZO film is grown by alternating between 15 ms pulses of diethylzinc (DEZ, Zn(C₂H₅)₂) and H₂O, and with periodic 15 ms pulses of Trimethylaluminum ((TMA), Al(CH₃)₃) as the aluminum dopant. Ultra- high purity continuous flowing

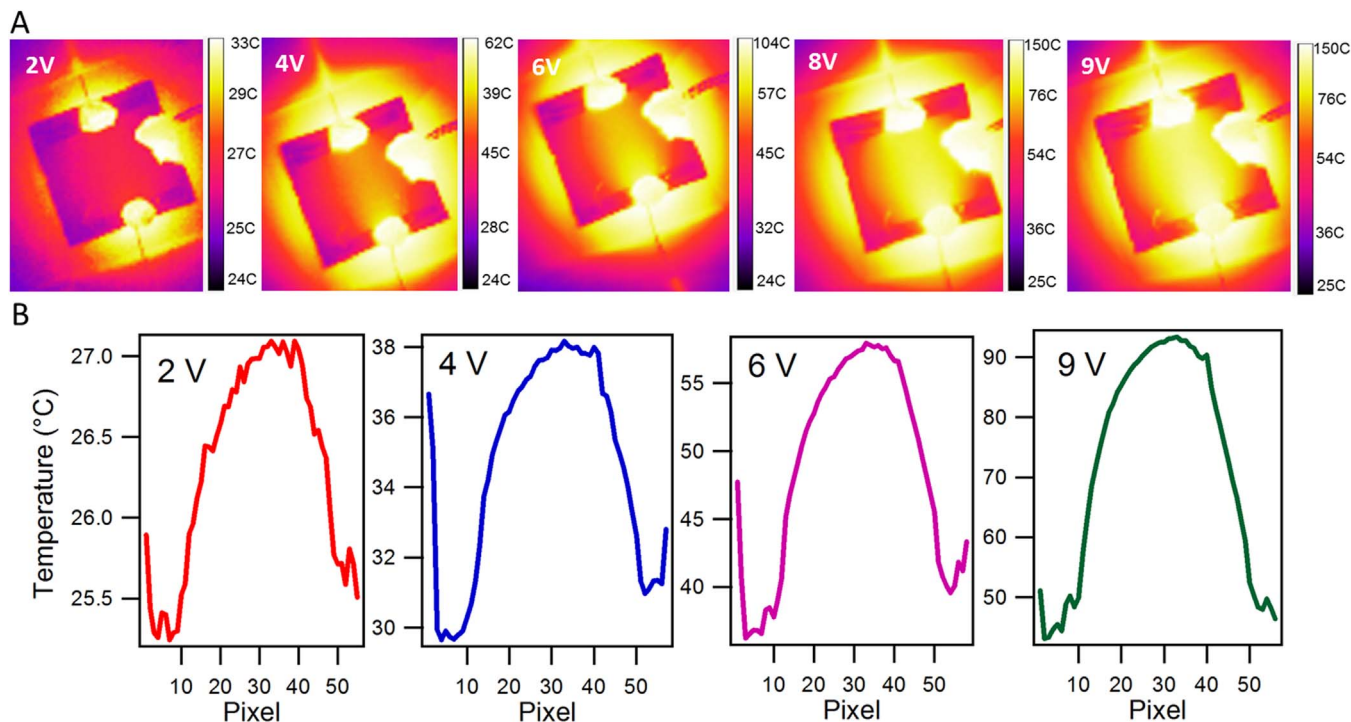


Figure 4 | Thermal imaging of the film during application of voltages. (A) The thermal imaging of the heat generated due to applied voltages using an infrared camera (320×240 pixel resolution) over a 1 cm² area of the AZO film. (B) The temperature profile across the top left to bottom right diagonal of the rectangular sample at different applied voltages up to 9 V.

N₂ purges the chamber in between precursor pulses. The purge time was 5 seconds. The substrate temperature was set to a desired substrate temperature. In our study, we varied the thickness of the AZO films by increasing the number of Zn : Al = 20 : 1 macrocycles. The structural and sequence arrangements are schematically illustrated (See schematics in Supplementary Fig. 1A).

The gradient film, G1, was grown by systematically varying the macrolayers (ML) from 60 to 15 ML as we fix Al = 1 and vary the ratio for Zn = 10, 20, 30 and 40, as schematically shown in Supplementary Fig. 1B. The number of total macrocycles was 2400 giving a thickness of approximately 280 nm. (See schematics in Supplementary Information Fig. 1B). The TOF-SIMS measurements confirm that the gradient sample contains less Al as the ratio changes from A : Zn = 1 : 10 to 1 : 40 (See Supplementary Information Fig. 1C).

Electro-absorption. The phenomenon of electric field induced change in absorption (electro-absorption), named the Franz-Keldysh effect^{27,28}, may be able to be experimentally seen in these AZO samples. If one considers the situation that an optical beam with frequency (ω) and a DC field are applied to the AZO sample, the total electric field is given by

$$E = E_0 + E_1 \cos(\omega t) \quad (3)$$

where E_0 and E_1 are the amplitudes of the DC and optical fields, respectively.

The polarization of the medium is given by

$$P = \epsilon_0 \chi^{(1)} E + \epsilon_0 \chi^{(2)} E E + \epsilon_0 \chi^{(3)} E E E + \dots \quad (4)$$

Substituting equation (3) into (4), we may obtain the polarization that determines the optical properties of the medium at frequency ω

$$P_1 = \epsilon_0 \left[\chi^{(1)}(\omega) + \chi^{(2)}(-\omega; 0, \omega) E_0 + \chi^{(3)}(-\omega; 0, 0, \omega) E_0^2 \right] E_1 \cos(\omega t) + \dots \quad (5)$$

Here only DC field related terms are given and the terms involving only the optical field are neglected since the light intensity was weak in our measurements.

Thus the effective permittivity of the medium is

$$\epsilon_{eff}(\omega, E_0) = \epsilon_L(\omega) + \sum_{j=2}^{\infty} \chi^{(j)} E_0^{j-1} \quad (6)$$

with

$$\epsilon_L(\omega) = 1 + \chi^{(1)}(\omega) = \epsilon_r(\omega) + i\epsilon_i(\omega) \quad (7)$$

The Drude-Sellmeier model was used to describe the linear permittivity $\epsilon_r(\omega)$ and $\epsilon_i(\omega)$ to obtain the Drude free-electron parameters of the thin film.

According to Drude theory, the imaginary part of the permittivity of the medium may be written as

$$\epsilon_i(\omega) = \frac{\Gamma \omega_p^2}{\omega(\omega^2 + \Gamma^2)} \quad (8)$$

while the real part is given by

$$\epsilon_r(\omega) = \epsilon_{\infty} - \frac{\omega_p^2}{\omega^2 + \Gamma^2} + \frac{B^2}{C^2 - \omega^2} \quad (9)$$

Here, ω_p and Γ are the free-electron plasma frequency and damping frequency, respectively. The first and third terms together provide a Sellmeier dispersion to describe the contribution from an off resonant interband transition. The background permittivity is represented by ϵ_{∞} . The second term in equation (5), $\chi^{(2)}(-\omega; 0, \omega) E_0$, is the so-called Pockels effect. The effective nonlinear susceptibility $\chi^{(2)}(-\omega; 0, \omega)$ describes the Pockels effect. The third term, $\chi^{(3)}(-\omega; 0, 0, \omega) E_0^2$, which depends on the square of the applied DC electric field, is the quadratic electro-optic effect (DC Kerr effect). The nonlinear susceptibility $\chi^{(n)}$ includes both real and imaginary parts.

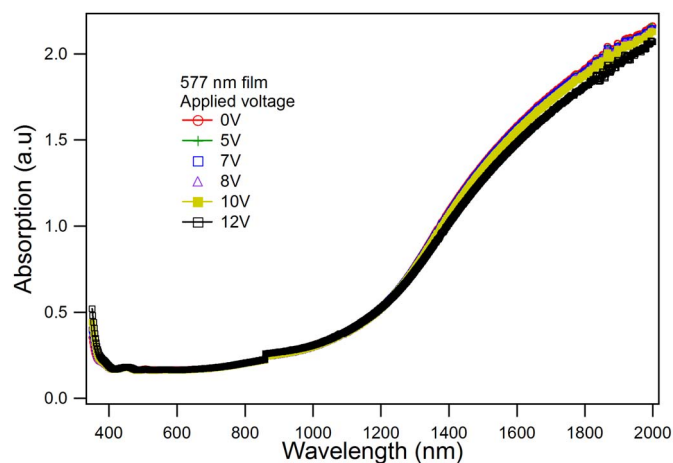


Figure 5 | Optical absorption as a function of wavelength at various applied voltages for the 577 nm thick AZO (Al : Zn = 1 : 20) film.



The real part leads to the above-mentioned electro-optic effects while the imaginary part contributes to changes in absorption of the medium. According to equation (6), the permittivity of the metamaterial can easily be controlled by the applied electric field. We found no significant electro-absorption change in 577 nm thick AZO thin films by simply changing the applied voltage on the sample as shown in Fig. 5. The slight decrease in the absorption is due to the thermal effects during the application of voltages.

- Pryce, I. M. *et al.* Highly strained compliant optical metamaterials with large frequency tunability. *NanoLett.* **10**, 4222 (2010).
- Smith, D. R., Pendry, J. B. & Wiltshire, M. C. K. Metamaterials and negative refractive index. *Science* **305**, 788–792 (2004).
- Rogacheva, A. V., Fedotov, V. A., Schwanecke, A. S. & Zheludev, N. I. Giant gyrotropy due to electromagnetic-field coupling in a bilayered chiral structure. *Phys. Rev. Lett.* **97**, 177401 (2006).
- Shalaev, V. M. Optical negative-index metamaterials. *Nat. Photonics* **1**, 41–48 (2007).
- Gansel, J. K. *et al.* Gold helix photonic metamaterial as broadband circular polarizer. *Science* **325**, 1513–1515 (2009).
- Chen, H.-T. *et al.* Active terahertz metamaterial devices. *Nature* **444**, 597–600 (2006).
- Tao, H., Strikwerda, A. C., Fan, K., Padilla, W. J., Zhang, X. & Averitt, R. D. Reconfigurable terahertz metamaterials. *Phys. Rev. Lett.* **103**, 147401 (2009).
- Dicken, M. J. *et al.* Frequency tunable near-infrared metamaterials based on VO₂ phase transition. *Opt. Express* **17**, 18330–18339 (2009).
- Soukoulis, C. M. & Wegener, M. Past achievements and future challenges in the development of three-dimensional photonic metamaterials. *Nat. Photonics* **5**, 523 (2011).
- Bhosle, V., Tiwari, A. & Narayan, J. Metallic conductivity and metal-semiconductor transition in Ga-doped ZnO. *Appl. Phys. Lett.* **88**, 032106 (2006).
- Bamiduro, O. *et al.* Metal-like conductivity in transparent Al: ZnO films. *Appl. Phys. Lett.* **90**, 252108 (2007).
- West, P. R. *et al.* Searching for better plasmonic materials. *Laser Photon. Rev.* **4**, 795 (2010).
- Boltasseva, A. & Atwater, H. A. Low-loss plasmonic metamaterials. *Science* **331**, 290 (2011).
- Naik, G. V. & Boltasseva, A. Semiconductors for plasmonics and metamaterials. *Physica Status Solidi, Rapid Research Letters* **4**, 295 (2010).
- Noginov, M. A. *et al.* Transparent conductive oxides: Plasmonic materials for telecom wavelengths. *Appl. Phys. Lett.* **99**, 021101 (2011).
- Naik, G. V., Kim, J. & Boltasseva, A. Oxides and nitrides as alternative plasmonic materials in the optical range. *Opt. Mater. Exp.* **1**, 1090 (2011).
- Naik, G. V. & Boltasseva, A. A comparative study of semiconductor-based plasmonic metamaterials. *Metamaterials* **5**, 1 (2011).
- Franzen, S. Surface plasmon polaritons and screened plasma absorption in indium tin oxide compared to silver and gold. *J. Phys. Chem. C* **112**, 6027 (2008).
- Dondapati, H., Santiago, K. & Pradhan, A. K. Influence of growth temperature on electrical, optical, and plasmonic properties of aluminum: zinc oxide films grown by radio frequency magnetron sputtering. *J. Appl. Phys.* **114**, 143506 (2013).
- Frolich, A. & Wegener M. Spectroscopic characterization of highly doped ZnO films grown by atomic-layer deposition for three-dimensional infrared metamaterials [Invited]. *Opt. Mater. Exp.* **1**, 883 (2011).
- Kim, H., Osofsky, M., Prokes, S. M., Glembocski, O. J. & Piqué, A. Optimization of Al-doped ZnO films for low loss plasmonic materials at telecommunication wavelengths. *Appl. Phys. Lett.* **102**, 171103 (2013).
- Mundle, R. M. *et al.* Electrical conductivity and photoresistance of atomic layer deposited Al-doped ZnO films. *J. Vac. Sci. Technol. A* **31**, 01A146 (2013).
- Noh, J.-Y., Kim, H., Kim, Y.-S. & Park, C. H. Electron doping limit in Al-doped ZnO by donor-acceptor interactions. *J. Appl. Phys.* **113**, 153703 (2013).
- Na, J.-S., Peng, Q., Scarel, G. & Parsons, G. N. Role of gas doping sequence in surface reactions and dopant incorporation during Atomic Layer Deposition of Al-Doped ZnO. *Chem. of Mater.* **21**, 5585 (2009).
- Lee, D.-J. *et al.* Structural and Electrical Properties of Atomic Layer Deposited Al-Doped ZnO Films. *Adv. Funct. Mater.* **21**, 448 (2011).
- Mundle, R. & Pradhan, A. K. Electrical response in atomic layer deposited Al: ZnO with varying stack thickness. *J. Appl. Phys.* **115**, 183503 (2014).
- Franz, W. Einfluss eines elektrischen feldes auf eine optische Absorptionskante. *Z. Naturforsch. Teil A* **13**, 484 (1958).
- Keldysh, L. V. Effects of a strong electric field on the optical properties of insulating crystals. *Zh. Eksp. Teor. Fiz.* **34**, 1138 (1958), *Sov. Phys. JETP* **7**, 788 (1958).
- Miller, D. A. B. *et al.* Electric field dependence of optical absorption near the band gap of quantum-well structures. *Phys. Rev. B* **32**, 1043 (1985).
- Miller, D. A. B., Chemla, D. S. & Schmitt-Rink, S. Relation between electroabsorption in bulk semiconductors and in quantum wells: The quantum-confined Franz-Keldysh effect. *Phys. Rev. B* **33**, 6976 (1986).
- Santiago, K., Mundle, R. M., Samantaray, C. B., Bahoura, M. & Pradhan, A. K. Nanopatterning of atomic layer deposited Al: ZnO films using electron beam lithography for waveguide applications in the NIR region. *Opt. Mater. Exp.* **2**, 1743 (2012).
- Duda, J. C., Hopkins, P. E., Shen, Y. & Gupta, M. C. Shapes of a suspended curly hair. *Phys. Rev. Lett.* **112**, 068103 (2013).
- Wu, Y. *et al.* Electrical transport and Al doping efficiency in nanoscale ZnO films prepared by atomic layer deposition. *J. Appl. Phys.* **114**, 024308 (2013).

Acknowledgments

We thank A. Lakhtakia (PSU) for fruitful discussions. We acknowledge financial support from the Department of Defense (DoD) Grant Number W911NF-11-1-0209, W911NF-11-1-0133 (US Army Research Office), and NSF-CREST (CNBMD) Grant number HRD 1036494. PH thanks Office of Naval Research Young Investigator Program Grant number N00014-13-4-0528. We would like to thank C. Donley (CHANL) for XPS measurements and related analysis. A link to the data reported here is included in the supplementary materials.

Author contributions

R.M. and K.S. carried out the synthesis, optical and electrical experiments and A.K.P., J.R.S., B.X., K.D.S., and M.B. performed the data analysis. R.C. and P.H. performed the thermal conductivity measurements. A.K.P. conceived the experiments and planned and supervised the project. All authors participated in the scientific discussions and manuscript preparation.

Additional information

Supplementary information accompanies this paper at <http://www.nature.com/scientificreports>

Competing financial interests: The authors declare no competing financial interests.

How to cite this article: Pradhan, A.K. *et al.* Extreme tunability in aluminum doped Zinc Oxide plasmonic materials for near-infrared applications. *Sci. Rep.* **4**, 6415; DOI:10.1038/srep06415 (2014).



This work is licensed under a Creative Commons Attribution-NonCommercial-NoDerivs 4.0 International License. The images or other third party material in this article are included in the article's Creative Commons license, unless indicated otherwise in the credit line; if the material is not included under the Creative Commons license, users will need to obtain permission from the license holder in order to reproduce the material. To view a copy of this license, visit <http://creativecommons.org/licenses/by-nc-nd/4.0/>